

R-matrix inner-shell electron-impact excitation of Fe¹⁵⁺ including Auger-plus-radiation damping

G Y Liang[‡], A D Whiteford and N R Badnell

Department of Physics, University of Strathclyde, Glasgow, G4 0NG, UK

Abstract. We present results for the inner-shell electron-impact excitation of Fe¹⁵⁺ using the intermediate-coupling frame transformation *R*-matrix approach in which Auger-plus-radiation damping has been included. The target and close-coupling expansions are both taken to be the 134 levels belonging to the configurations $2s^2 2p^6 3l$, $2s^2 2p^5 3s 3l$, $2s^2 2p^5 3p^2$ and $2s^2 2p^5 3p 3d$. The comparison of Maxwell-averaged effective collision strengths with and without damping shows that the damping reduction is about 30-40% for many transitions at low temperatures, but up to 80% for a few transitions. As a consequence, the results of previous Dirac *R*-matrix calculations (Aggarwal and Keenan, 2008) overestimate the effective collision strengths due to their omission of Auger-plus-radiation damping.

Submitted to: *J. Phys. B: At. Mol. Opt. Phys.*

[‡] E-mail: guiyun.liang@strath.ac.uk

PACS numbers: 34.80 Kw

1. Introduction

Radiation from Fe^{15+} occupies a considerable fraction of the EUV and X-ray radiation spectrum of (the astrophysically abundant element) iron. Its temperature of peak fractional abundance is at $\approx 2.5 \times 10^6$ K in collision dominated plasmas (Bryans *et al* 2006) and a few times 10^4 K in photoionized plasmas (Kallman and Bautista 2001). Observations of inner-shell excitation lines such as $2p^63s-2p^53l3l'$ in the solar corona have led to extensive investigations of inner-shell excitation data for this ion (see, e.g., Dere *et al* 2001).

Earlier calculations adopted the distorted-wave (DW) approximation. For example, Cornille *et al* (1994) reported excitation data amongst the lowest 44 levels belonging to the $2p^63s$ and $2p^53s3l$ ($l=s, p$ and d) configurations. This data was adopted by Phillips *et al* (1997) to analyze the contribution of satellite lines to line-ratios, arising from inner-shell excitations, which are useful in solar diagnostic applications. Resonant-excitation plays an important role in electron-ion collision processes, enhancing the effective collision strength (Υ), especially for forbidden transition lines. These lines are usually density- and temperature-sensitive and so have potential diagnostic applications. Bautista (2000) performed a standard R -matrix (Berrington *et al* 1995) calculation for inner-shell excitation which included the 134-levels belonging to the $2s^22p^63l$, $2s^22p^53s3l$, $2s^22p^53p^2$ and $2s^22p^53p3d$ ($l=s, p$ and d) configurations (the same configurations considered in the present work). The enhancement of Maxwell-averaged effective collision strengths (Υ) by resonances in the ordinary collision strengths (Ω) was found to be up to three orders of magnitude at low temperatures, for some transitions. In Bautista's calculation, relativistic effects were included by using term-coupling coefficients (TCC) via the JAJOM code §. This changed the background collision strengths by up to an order of magnitude when compared to the results of his LS -coupling calculations, in which the algebraic splitting of scattering matrices was used to obtain the fine-structure data. Recently, Aggarwal & Keenan (2008) calculated inner-shell excitation data using the same 134-level target configurations with the fully-relativistic Dirac atomic R -matrix code (DARC) of Norrington and Grant (1987). Detailed comparisons with the excitation data of Bautista (2000) were made, and they pointed out deficiencies in the data of Bautista due to the methodology used by JAJOM.

In a detailed study of Fe^{14+} , Berrington *et al* (2005) found that the Breit–Pauli R -matrix effective collision strengths agreed with the DARC calculations to within 6%. For complex species, the number of (closely spaced) levels that must be included in the close-coupling (CC) expansion is very large, which makes the calculation computationally demanding. An alternative approach to a full Breit–Pauli R -matrix calculation is to perform an R -matrix calculation in LS -coupling and then, on making use of multi-channel quantum defect theory (MQDT), transform the resulting ‘unphysical’ K -

§ The TCCs were obtained from the R -matrix RECUPD code.

or S -matrices to intermediate coupling. This eliminates at root the deficiency of JAJOM, viz. only transforming the open–open part of the physical K -matrix, since all channels are treated as being ‘open’ in MQDT. This is the intermediate coupling frame transformation (ICFT) method. In studying of the ICFT R -matrix electron excitation of Fe^{14+} and Ni^{4+} , Griffin *et al* (1998) and Badnell & Griffin (1999) found that the ICFT results agreed closely with those determined from the full Breit-Pauli R -matrix calculation. Another advantage of the ICFT method is the saving of computational time, which makes meaningful iso-electronic sequence calculations a reality within the R -matrix framework (Witthoeft *et al* 2007).

Resonances superimposed upon the background cross section enhance the effective collision strengths for electron-impact excitation, especially at lower temperatures and/or for weaker transitions. However, some resonant states may decay by an Auger process or fluorescence radiation and so are lost to the transition under study. Such loss mechanisms can be represented by a complex optical potential. Robicheaux *et al* (1995) provided a detailed description of radiation damping via such a potential within the R -matrix method. Subsequently, Gorczyca *et al* (1995) showed the effect of radiation damping on the electron-impact cross section of Ti^{20+} while Gorczyca & Badnell (1996) demonstrated its even greater importance for photorecombination. Gorczyca and Robicheaux (1999) extended the optical potential approach so as to include Auger damping. Whiteford *et al* (2002) demonstrated the Auger damping effect on the effective collision strengths of inner-shell transitions in Li-like Ar^{15+} and Fe^{23+} , and showed significant reductions in effective collision strengths at low temperatures ($\sim 30\%$ for the $1s^2 2s^2 \ ^2S_{1/2} - 1s 2s^2 \ ^2S_{1/2}$ transition of Fe^{23+}). Correspondingly, this has an influence on the spectroscopic diagnostic and modelling of plasmas, especially photoionized plasmas which typically have a much lower electron temperature. Furthermore, Bautista *et al* (2004) demonstrated the smearing of the photoabsorption K-edge by such damping, primarily Auger, for Fe^{16+} through Fe^{22+} .

In the present work we study the inner-shell electron-impact excitation of Fe^{15+} , via the R -matrix ICFT approach, using the same CC and CI expansions as in the work of Aggarwal & Keenan (2008) but now include Auger-plus-radiation damping. This work is a part of on-going collaborative work — the UK atomic processes for astrophysical plasmas (APAP) network||, a broadening of scope of the original UK RmaX network. In section 2 we present details of our structure calculation and make comparisons with other data available in the literature. Our calculations for the scattering problem are detailed in section 3. The results, and their comparison with those of others, are discussed in section 4. We conclude with section 5.

2. Structure

We included the following configurations: $2s^2 2p^6 3l$, $2s^2 2p^5 3s 3l$, $2s^2 2p^5 3p^2$ and $2s^2 2p^5 3p 3d$. The orbital basis functions ($1s - 3d$) were obtained from AUTOSTRUCTURE

|| http://amdpp.phys.strath.ac.uk/UK_APAP

(Badnell 1986) using the Thomas-Fermi-Dirac-Amaldi model potential (Eissner *et al* 1974). The radial scaling parameters were obtained by a two-step procedure of energy minimization. In the first step, the average energy of all 59 terms was minimized by allowing all scaling parameters (one for each nl orbital) to change. We then fixed the resulting radial scaling parameter of the 1s orbital ($\lambda_{1s}=1.41958$). Finally, we minimized the average energy sum of all 134 levels, obtained from an intermediate coupling calculation, so as to determine the remaining scaling parameters. The resultant values are $\lambda_{2s}=1.30324$, $\lambda_{2p}=1.14032$, $\lambda_{3s}=1.23627$, $\lambda_{3p}=1.13555$ and $\lambda_{3d}=1.00615$. (The mass-velocity plus Darwin contribution from the 1s orbital is too large for the minimization procedure to converge if the 1s scaling parameter is varied in intermediate coupling — the energy functional has no minimum.)

We compare our energies with the values available from the NIST database v3.0 ¶ and the GRASP calculation of Aggarwal & Keenan (2007) (hereafter referred to as AK07). Their (AK07) calculations of structure used the same configurations as herein. The subsequent electron collision scattering calculations of Aggarwal & Keenan 2008 (hereafter, AK08) also used a structure determined by AK07. Excellent agreement (within 0.1%) is obtained when compared with the results of the AK07 GRASP calculation that omitted Breit and QED effects. The AK07 data is systematically higher than our results by less than 0.1 Ryd for the doubly-excited levels. The agreement with the NIST data is to within 0.5%, except for the $2s^2 2p^5 3s 3d$ $^2D_{5/2}$, $^2F_{7/2}$, $^2F_{5/2}$ and $^2P_{3/2}$ levels. The difference is within 0.2% for these levels. Note, although AK07 obtained better agreement with the NIST data when Breit and QED effects were included, they are not present within DARC (nor two-body fine-structure within Breit–Pauli R -matrix) and so such a structure cannot be used in a scattering calculation.

Due to the strong configuration interaction and level mixing, as illustrated in table 1 of AK07, level orderings for comparisons are not same in different calculations. Here, we match the level assignment according to configuration, total angular momentum and then energy ordering. Fortunately, only a few level assignments are inconsistent in the two different calculations, which facilitates our later comparisons for radiative decay rates (A -coefficients) and collision strengths. However, for some levels, their different assignments result in large discrepancies (up to 0.84 Ryd) with the NIST values in the AK07 work, such as for levels 11 and 14. Similar disturbed level ordering appears for levels 19/20, 26/27, 62/63 etc. Our new assignment eliminates the mis-order compared to the NIST values, as shown in table 1.

We also performed a structure calculation with the flexible atomic code (FAC) of Gu (2003), which shows slightly better agreement with our AUTOSTRUCTURE results than those from GRASP. Both are systematically higher than GRASP's, FAC more so. The results of the three different calculations are compiled in table 1, along with NIST data.

In the scatter plot of figure 2, we compare radiative decay rates ($A_{i,j}$ for the

¶ http://physics.nist.gov/PhysRefData/ASD/levels_form.html

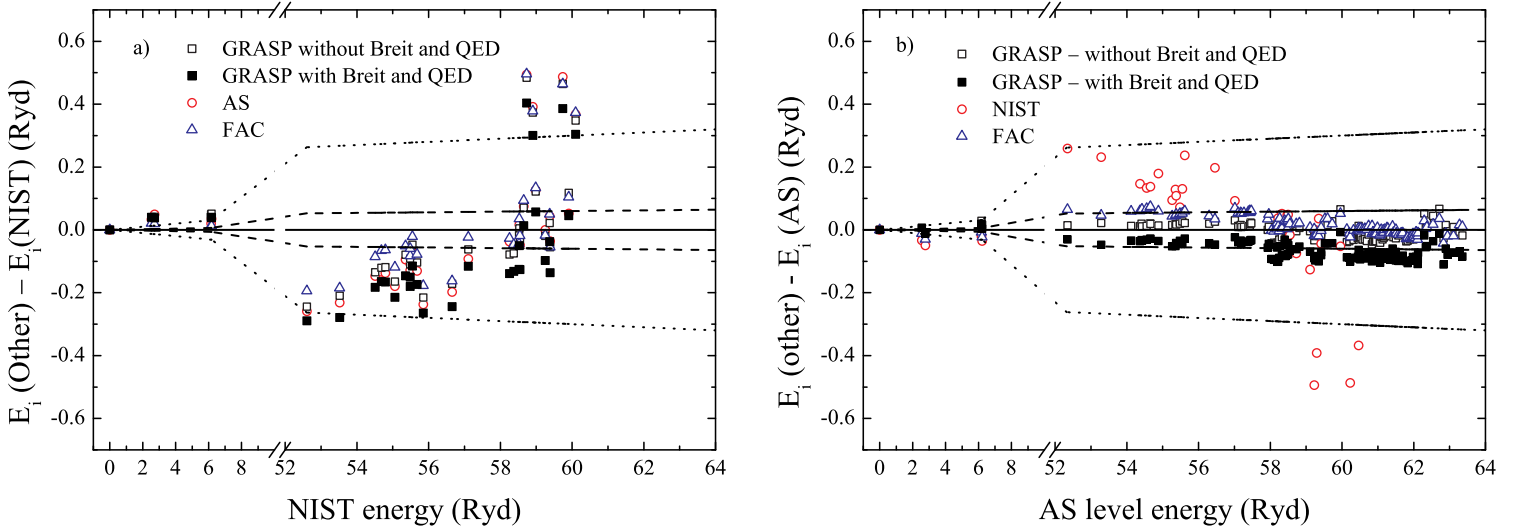


Figure 1. Comparisons of energy levels from the present AUTOSTRUCTURE (AS), GRASP (Aggarwal & Keenan, 2007) and FAC (present work) calculations. a): differences relative to the available experimental values (NIST database) versus the NIST data. Opened and filled square symbols correspond to the GRASP results, without and with the inclusion of Breit and QED effects, respectively (Aggarwal & Keenan 2007); triangle symbols indicate the present FAC results; opened circles denote the present AS results. b): The differences relative to the present AS results versus the present AS results. Symbols as before. The dashed and dotted lines correspond to agreement within 0.1% and 0.5%, respectively. [Colour online]

$i \leftarrow j$ transition) for all electric and magnetic multipoles from our AUTOSTRUCTURE calculation with the GRASP data from AK07 for decays to the lowest 5-lying levels. Electric dipole line strengths are also shown. Rates for some electric dipole transitions to the ground state are listed in table 2. For two-thirds of the transitions, the results of the two calculations agree to within 20%, and 95% of transitions agree to within a factor of 2. We also note that there are differences of more than a factor of 2, and up to an order of magnitude for few transitions, which may be due to the mis-match of the mapping of energy levels according to the parity, total angular momentum and energy order scheme in the two different calculations. Overall, the agreement is satisfactory.

3. Scattering

For the present case of Fe^{15+} , the resonance state configurations are of the form $[2s, 2p]^{q-1}[3s, 3p, 3d]^2nl$ (here $q = 8$, $n \geq 3$), and they can decay via the following channels

$$[2s, 2p]^{q-1}[3s, 3p, 3d]^2nl \rightarrow [2s, 2p]^q[3s, 3p, 3d] + e^- \quad (1)$$

$$\rightarrow [2s, 2p]^qnl + e^- \quad (2)$$

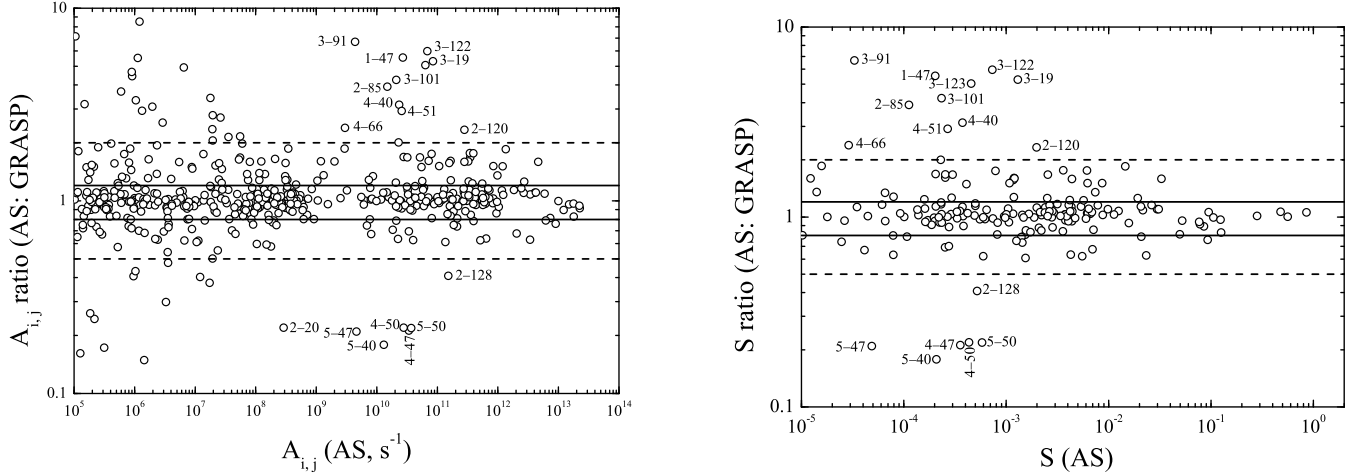


Figure 2. Comparison of radiative decay rates, $A_{i,j}$, (all multipoles) and electric dipole line strengths (S) from the present AUTOSTRUCTURE (AS) calculation and the GRASP calculation by Aggarwal & Keenan (2007) for transitions to the lowest 5 levels. Solid and dashed lines correspond to agreement within 20% and a factor of 2, respectively. Transitions with differences of more than a factor of 2 are marked by the transition label. (In the case of the rates, labelling is restricted to strong rates: $\gtrsim 10^9 \text{ s}^{-1}$.)

$$\rightarrow [2s, 2p]^q [3s, 3p, 3d]^2 + h\nu \quad (3)$$

$$\rightarrow [2s, 2p]^q [3s, 3p, 3d]nl + h\nu . \quad (4)$$

The participator LMn Auger pathway (1) scales as n^{-3} and is automatically described in the R -matrix method by the contribution to the close-coupling expansion from the right hand side of (1). However, the spectator LMM Auger pathway (2) is independent of n and only low- n resonances ($n \leq 3$ here) can be included in the close-coupling expansion. But, the spectator Auger pathway dominates for $n > 3$. The last two channels, (3) and (4), represent radiation damping. These Auger and radiation damping processes reduce the resonant-enhancement of the excitation collision strengths and can be expected to be especially important for inner-shell transitions due to the large energy jump.

For the Auger process, the participator Auger channel can be included explicitly within the R -matrix close-coupling expansion, whereas the spectator Auger decay cannot easily be included for the higher- n resonances as it requires the inclusion of target states with nl (with $n > 3$) orbitals. (So, only the Auger damping from $n = 3$ resonances has been included in the work of AK08).

We employ the R -matrix intermediate-coupling frame transformation (ICFT) method of Griffin *et al* (1998) allowing for both Auger-plus-radiation damping via the complex optical potential, as described above. We used 25 continuum basis per orbital angular momentum. Contributions from partial waves up to $J=12$ were included in the exchange calculation. The contributions from higher partial waves up to $J=42$ were

included via a non-exchange calculation. A ‘top-up’ was used to complete the partial collision strength sum over higher J -values by using the Burgess sum rule (Burgess 1974) for dipole transitions and a geometric series for the non-dipole transitions (Badnell & Griffin 2001). In the outer-region calculation, we used an energy mesh step of $2 \times 10^{-6} z^2$ Ryd through the resonance region (from threshold to 72 Ryd), where z is the residual charge of the ion (15 in the present case). Beyond the resonance region (from 72 to 450 Ryd), for the exchange calculation, an energy step of $2 \times 10^{-4} z^2$ Ryd was used. For the non-exchange calculation, we used a step of $1 \times 10^{-3} z^2$ Ryd over the entire energy range. The calculation was carried-out up to an incident energy of 450 Ryd. We used the infinite energy Born limits (non-dipole allowed) and line-strengths (dipole-allowed) from AUTOSTRUCTURE so that the collision strengths could be interpolated at any desired energy when Maxwell-averaging (see Whiteford *et al* 2001).

Observed energies were used for the lowest 25-lying levels. For those levels missing from the NIST database, we first derived the mean value of differences between our level energies and the corresponding NIST values for available levels of the $2s^2 2p^5 3s 3p$ configuration, then we adjusted our calculated level energies by this mean value. These observed and adjusted energies are employed in the MQDT formula which converts from the slowly-varying-with-energy unphysical K -matrix to the strongly (resonant) energy-dependent physical K -matrix. This ensures that Rydberg series of resonances converge on the observed thresholds. In addition, low-lying (non-correlation) resonances can be expected to be positioned accurately just above excitation thresholds. A similar procedure has been demonstrated to be very accurate in the study of dielectronic recombination, where there is much precise experimental cross section data with which to compare with (see Savin *et al* 2002, for example).

In figure 3, we show the collision strength of the $2s^2 2p^6 3s \ ^2S_{1/2} - 2s^2 2p^5 3s^2 \ ^2P_{3/2}$ transition line, both without damping⁺ as well as with Auger-plus-radiation damping. The reduction due to the effect of Auger-plus-radiation damping is very apparent on resonances, especially at higher energies, and can be up to two orders of magnitude. Some resonances are completely damped. The damping is dominated by far ($\sim 90\%$) by the Auger process for $n > 3$. We also performed a distorted-wave (DW) calculation by using the FAC code with the same configuration interactions as in our 134-level ICFT R -matrix calculation. For this 1–6 transition, the DW data is lower than the background value obtained from R -matrix by 25% at 8 Ryd.

Generally speaking, Maxwell-averaged effective collision strengths (Υ) have a more extensive application than the ordinary collision strengths (Ω), in addition to the advantage of a much smaller storage size. Test calculations show that the effective collision strengths have converged (to within 1% for 87% of transitions) down to a temperature of 5.12×10^4 K on using an energy mesh step of $2 \times 10^{-6} z^2$ Ryd. At high temperatures, effective collision strengths have converged on using a much coarser mesh step of $5 \times 10^{-6} z^2$ Ryd. So, in our following work, we adopt an energy step of

⁺ Of course, $n = 3$ Auger damping is still present here as it is intrinsic to the close-coupling expansion.

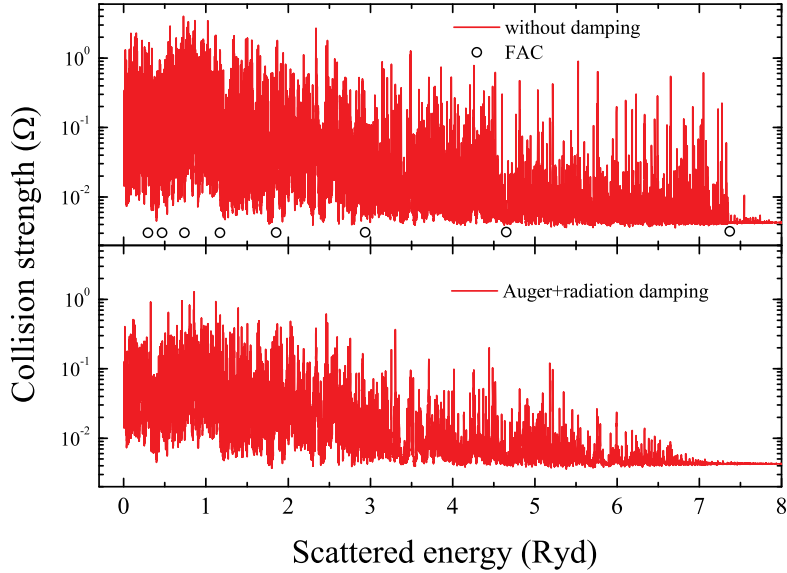


Figure 3. ICFT R -matrix excitation collision strengths for the $2s^2 2p^6 3s \ ^2S_{1/2} - 2s^2 2p^5 3s^2 \ ^2P_{3/2}$ transition, without damping (top) and Auger-plus-radiation damping (bottom). The circle symbols represent the results of our FAC DW calculation. [Colour online]

$2 \times 10^{-6} z^2$ Ryd, which is smaller than that adopted by AK08, by a factor of 2.

4. Results and Discussions

4.1. Comparison of undamped results: ICFT R -matrix vs DARC

We make comparison with the results of AK08 calculated by using DARC. We make contrasting comparisons at a low temperature (5.12×10^4 K) and a high one (1.58×10^7 K) as shown in figure 4, in which transitions from the lowest 5-lying levels to all higher levels (total 655 transitions) are plotted for dipole allowed (211) and non-dipole allowed (426) transitions. In intermediate coupling, spin-orbit mixing means that very few transitions that were forbidden in LS -coupling remain so. Instead, they have small but non-zero line strengths or infinite energy Born limits. Indeed, only 18 transitions from the lowest 5-lying levels are strictly forbidden according to this definition (and are not shown in figure 4).

For most transitions, our undamped ICFT R -matrix results agree with the DARC ones of AK08, to within 20% over the entire temperature range. At the low temperature (5.12×10^4 K), there are 35.5% of dipole and 20.7% of non-dipole allowed transitions with a difference of over 20%. This difference decreases to 25.1% of dipole and 13.8% of non-dipole allowed transitions at the high temperature (1.58×10^7 K) at the low temperature (5.12×10^4 K). Here, for dipole transitions, we find that there is a strong correlation

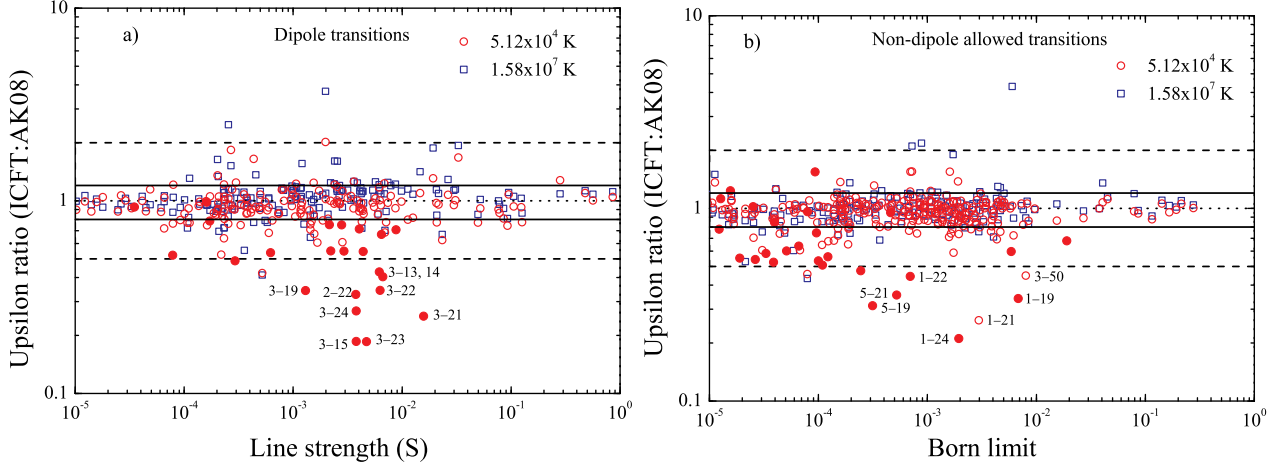


Figure 4. Scatter plot of ratios of ‘undamped’ effective collision strengths from the present ICFT R -matrix calculation and the DARC calculation of Aggarwal & Keenan (2008) as a function of present AS a) line strength (S) (for dipole transitions) and b) Born-limit (non-dipole allowed transitions). “o” and “•” symbols denote transitions at 5.12×10^4 K with threshold energy differences between ICFT and AK08 calculations being less than and greater than 0.2 Ryd, respectively. “□” symbols: corresponding results at 5.12×10^7 K. Solid and dashed lines correspond to agreement within 20% and a factor of 2, respectively. Dotted lines mark where the ratios agree. [Colour online]

between the ratio of the ICFT to DARC Υ values and the ratio of the AS to GRASP line strengths. The ICFT/DARC agreement for non-dipole allowed transitions should also be strongly correlated with the atomic structure — this time for the infinite energy Born limit, but we do not have such results for GRASP.

In figure 4, we identify a group of dipole and non-dipole allowed transitions (see table 3) for which the ratio of line strengths (electric dipole only) is close to unity but the DARC effective collision strengths are systematically larger than those obtained from ICFT, at the lower temperature. This is probably due to the smaller excitation energies used by AK08 (recall, we adjusted to observed) which means that there are additional resonances present at lower energies/temperatures in the AK08 data. This can be tested indirectly by looking at excitations to higher levels, which also have strong resonant contributions. For example, for the 1–28 transition (not shown) with a threshold energy difference of 0.041 Ryd, the Υ values are 7.58×10^{-3} and 7.61×10^{-3} , respectively, at the low temperature.

AK08 selected the 1–15 and 1–21 transitions to reveal inadequacies of term-coupling via the JAJOM code, as used by Bautista (2000), which results in the sudden increase and/or decrease of background collision strengths when relativistic effects are included for some transitions (see figure 3 in Bautista (2000) and the bottom two panels in figure 5). This is exactly the same inadequacy demonstrated originally by Griffin *et al* (1998) when they introduced the ICFT R -matrix method to solve the problem,

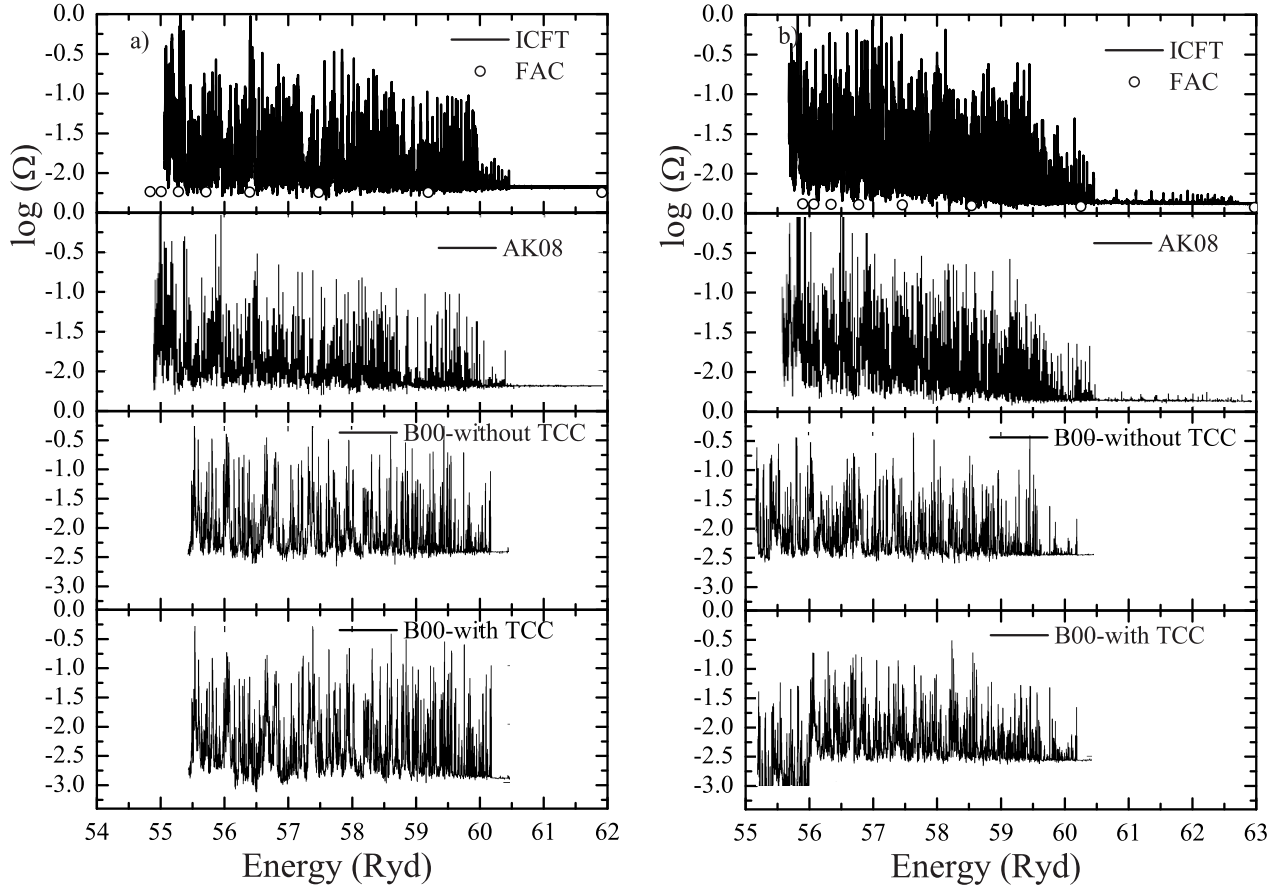


Figure 5. Collision strengths (Ω) from the ICFT R -matrix (present work), DARC (AK08) and JAJOM (Bautista (2000): B00) calculations. a): for 1–15 ($2s^22p^63s\ ^2S_{1/2}-2s^22p^53s3p\ ^2S_{1/2}$) transition line. b): 1–21 ($2s^22p^63s\ ^2S_{1/2}-2s^22p^53s3p\ ^2D_{5/2}$) transition line. “o” denote DW values obtained from FAC (present work).

without resorting to a full Breit–Pauli (or Dirac) calculation. AK08 conclude that this inadequacy is the reason for the large discrepancies between the results of their two calculations. In order to illustrate the inadequacy of the JAJOM method and the overestimation of AK08 at the lower temperature for some transitions (see filled circles in figure 4-a), we compare the underlying collision strengths for 1–15 and 1–21 transitions in figure 5. We see that the background does not shift down and no sudden jumps appear in the present ICFT results, in contrast to that seen from JAJOM — see the bottom two panels of figure 5. The background of ICFT Ω -values show excellent agreement with the DARC ones. Our DW results obtained from FAC are also overlapped, showing an excellent agreement with the background result of the two R -matrix calculations. Additionally, the resonance structures in the two R -matrix calculations basically agree with each other. However, because the energy of $2s^22p^53s3p\ ^2S_{1/2}$ (15-) and $^2D_{5/2}$ (21-) levels of the AK08’s data are lower than the observed values which we use, by ≈ 0.2 Ryd,

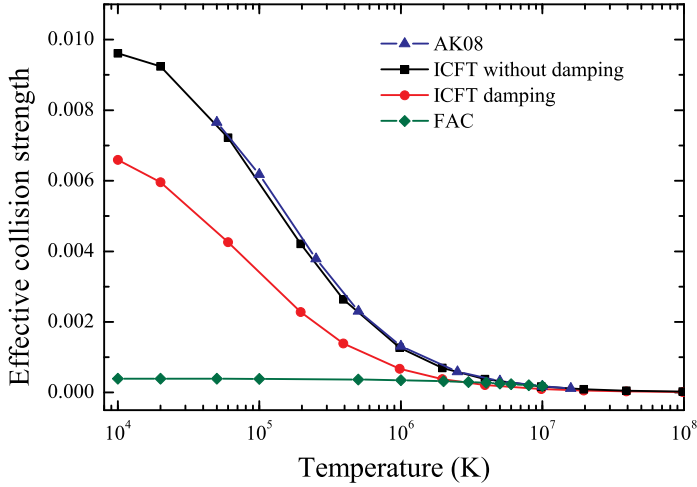


Figure 6. Comparison of the effective collision strengths for the $2s^2 2p^6 3s^2 S_{1/2} - 2s^2 2p^5 3p^2 ^4P_{5/2}$ transition (1 – 28). ICFT R -matrix and FAC DW are present results. AK08 denotes the DARC results of Aggarwal & Keenan (2008). [Colour online]

resonances around this region appear in the work of AK08, as shown in figure 5. So, their results are probably somewhat of an overestimate of the effective collision strengths at lower temperatures.

4.2. Comparison of ICFT R -matrix results: damped vs undamped

Figure 6 shows the results of several calculations of the effective collision strength (Υ) for the $2s^2 2p^6 3s^2 S_{1/2} - 2s^2 2p^5 3p^2 ^4P_{5/2}$ transition (1 – 28). They demonstrate the physics we seek to describe: firstly, on comparing R -matrix results with our DW ones obtained with FAC, we see that the resonant enhancement is about a factor of 8 at 2×10^4 K (typical of where Fe^{15+} is abundant in photoionized plasmas); secondly, there is close agreement between our present undamped ICFT R -matrix results and the DARC R -matrix ones of AK08; finally, Auger-plus-radiation damping lowers the resonance enhanced results by nearly a factor of 2, again at 2×10^4 K.

The widespread effect of Auger-plus-radiation damping is illustrated via a scatter plot of the ratios of damped to undamped Υ values for dipole (figure 7-a), non-dipole allowed (figure 7-c) and forbidden (figure 7-e) transitions. We see that the reduction at the low temperature (5.12×10^4 K) can be up to a factor of 3 for a few (1.3%) dipole transitions. The effect reduces with increasing of temperature and is less than 10% for 97.5% of these transitions at the high temperature (5.12×10^7 K). An illustrative way to quantify the information in the scatter plot is to count how many transitions differ by more than a given amount. In figure 7-b, we show the percentage of each class of transition where the damping effect is at least 5%, 10%, 15%, 20% and 30%. About 20% of dipole transitions show a damping effect of more than 30% at 5.12×10^4 K.

At higher temperatures, the damping becomes a smaller effect — less than 6% of dipole transitions show a >30% effect at 2.56×10^6 K, for example. For non-dipole allowed transitions (see figure 7-c), the damping effect can be up to a factor 3 for some transitions (2.1%) with a Born limit between 10^{-4} and 10^{-2} at the low temperature (5.12×10^4 K). The effect reduces to less than 10% for 88.7% of these transitions at the high temperature (5.12×10^7 K). Counting statistics (see figure 7-d) reveals that $\approx 25\%$ of non-dipole allowed transitions show a reduction more than 30% at the low temperature. There are only a few forbidden transitions (1.6% of the 8911 transitions in total). The damping effect is stronger for weaker excitations, see figure 7-e. About 44% of forbidden transitions show a damping effect over 30% at the low temperature (5.12×10^4 K) — see figure 7-f. At the high temperature, the percentage is still 40% of forbidden transitions with damping over 10%. This value is significantly higher than that for dipole (2.5%) and non-dipole allowed (11.3%) transitions. We also note that the forbidden transitions are affected over a wider range of electron temperatures.

Finally, in table 4, the undamped and damped effective collision strengths are given for excitations from the ground level at three temperatures of 5.12×10^4 , 5.12×10^5 , and 5.12×10^6 K. The full set of data (energy levels, radiative rates and effective collision strengths) are made available through different archives and databases (the Oak Ridge Controlled Fusion Atomic Data Center (CFADC)* in the ADAS *adf04* format (Summers 2004), ADAS‡ and CHIANTI††).

5. Conclusions

The level-resolved inner-shell electron-impact excitation of Fe^{15+} has been studied via the intermediate coupling frame transformation R -matrix method which can allow for the inclusion of Auger-plus-radiation damping of such resonantly-excited states. The 134 levels belonging to the configurations $2s^2 2p^6 3l$, $2s^2 2p^5 3s 3l$ ($l=s, p$ and d), $2s^2 2p^5 3p^2$ and $2s^2 2p^5 3p 3d$ were included in both the target configuration and close-coupling expansions. A comparison of energy levels and radiative rates with those of Aggarwal & Keenan (2007) reveals the target structures to be comparable, and so form the basis for comparison with the excitation data of Aggarwal & Keenan (2008).

The results of our undamped ICFT R -matrix calculation agree well with the undamped DARC effective collision strengths of Aggarwal & Keenan (2008) for most excitations. For a few transitions, their results are higher than ours by a factor of two at low temperatures. This is probably due to their use of smaller theoretical transition energies than ours, which were adjusted to the observed values. When Auger-plus-radiation damping is included, our results are systematically smaller than those of Aggarwal & Keenan (2008). Moreover, the reduction can be up to a factor of 3 for some transitions. The number of transitions where the reduction of Υ exceeds

* http://www-cfadc.phy.ornl.gov/data_and_codes

‡ <http://www.adas.ac.uk/>

†† <http://www.chianti.rl.ac.uk/>

20% occupies 30.2%, 37.7% and 70.7% of dipole, non-dipole allowed and forbidden transitions, respectively, at the low temperatures typical of where Fe¹⁵⁺ is abundant in photoionized plasmas.

In summary, Auger-plus-radiation damping plays an important role on the electron-impact excitation of inner-shell transitions. Thus, for many transitions, the results of previous undamped inner-shell calculations overestimate the effective collision strengths significantly.

6. Acknowledgments

The work of the UK APAP program is funded by the UK STFC under grant no. PP/E001254/1 with the University of Strathclyde. One of us (GY) would like to thank M. C. Witthoef for some helpful discussions.

References

- [1] Aggarwal K M and Keenan F P 2007 *Astron. Astrophys.* **463** 399
- [2] Aggarwal K M and Keenan F P 2008 *J. Phys. B: At. Mol. Opt. Phys.* **41** 015701
- [3] Badnell N R 1986 *J. Phys. B: At. Mol. Opt. Phys.* **19** 3827
- [4] Badnell N R and Griffin D C 1999 *J. Phys. B: At. Mol. Opt. Phys.* **32** 2267
- [5] Badnell N R and Griffin D C 2001 *J. Phys. B: At. Mol. Opt. Phys.* **34** 681
- [6] Bautista M A 2000 *J. Phys. B: At. Mol. Opt. Phys.* **33** 71
- [7] Bautista M A, Mendoza C, Kallman T R and Palmeri P 2004 *Astron. Astrophys. Suppl.* **418** 1171
- [8] Berrington K A, Ballance C P, Griffin D C and Badnell N R 2005 *J. Phys. B: At. Mol. Opt. Phys.* **38** 1667
- [9] Berrington K A, Eissner W and Norrington P N 1995 *Comput. Phys. Commun.* **92** 290
- [10] Bryans P, Badnell N R, Gorczyca T W, Laming J M, Mitthumsiri W and Savin D W 2006 *Astrophys. J. Suppl.* **167** 343
- [11] Burgess A 1974 *J. Phys. B: At. Mol. Opt. Phys.* **7** L364
- [12] Cornille M, Dubau J, Faucher P, Bely-Dubau F and Blancard C 1994 *Astron. Astrophys. Suppl.* **105** 77
- [13] Dere K P, Landi E, Young P R and Del Zanna G 2001 *Astrophys. J. Suppl.* **134** 331
- [14] Eissner W, Jones M and Nussbaumer H 1974 *Comput. Phys. Commun.* **4** 270
- [15] Gorczyca T W and Badnell N R 1996 *J. Phys. B: At. Mol. Opt. Phys.* **29** L283
- [16] Gorczyca T W and Robicheaux F 1999 *Phys. Rev. A* **60** 1216
- [17] Gorczyca T W, Robicheaux F, Pindzola M S and Badnell N R 1995 *Phys. Rev. A* **52** 3852
- [18] Griffin D C, Badnell N R and Pindzola M S 1998 *J. Phys. B: At. Mol. Opt. Phys.* **31** 3713
- [19] Gu M F 2003 *Astrophys. J.* **582** 1241
- [20] Kallman T and Bautista M 2001 *Astrophys. J. Suppl.* **133** 221
- [21] Norrington P H and Grant I P 1987 *J. Phys. B: At. Mol. Opt. Phys.* **20** 4869
- [22] Phillips K J H, Greer C J, Bhatia A K, Coffey I H, Barnsley R and Keenan F P 1997 *Astron. Astrophys.* **324** 381
- [23] Robicheaux F, Gorczyca T W, Pindzola M S and Badnell N R 1995 *Phys. Rev. A* **52** 1319
- [24] Savin D W, Behar E, Kahn S M, Gwinner G, Saghir A A, Schmitt M, Grieser M, Repnow R, Schwalm D, Wolf A, Bartsch T, Müller A, Schippers S, Badnell N R, Chen M H and Gorczyca T W 2002 *Astrophys. J. Suppl.* **138** 337
- [25] Summers H P 2004 *The ADAS User Manual* version 2.6 (<http://adas.phys.strath.ac.uk>)
- [26] Witthoef M C and Badnell N R 2008 *Astron. Astrophys.* **481** 543

- [27] Whiteford A D, Badnell N R, Ballance C P, O'Mullane M G, Summers H P and Thomas A L 2001 *J. Phys. B: At. Mol. Opt. Phys.* **34** 3179
- [28] Whiteford A D, Badnell N R, Ballance C P, Loch S D, O'Mullane M G and Summers H P 2002 *J. Phys. B: At. Mol. Opt. Phys.* **35** 3729
- [29] Witthoeft M C, Whiteford A D and Badnell N R 2007 *J. Phys. B: At. Mol. Opt. Phys.* **40** 2969

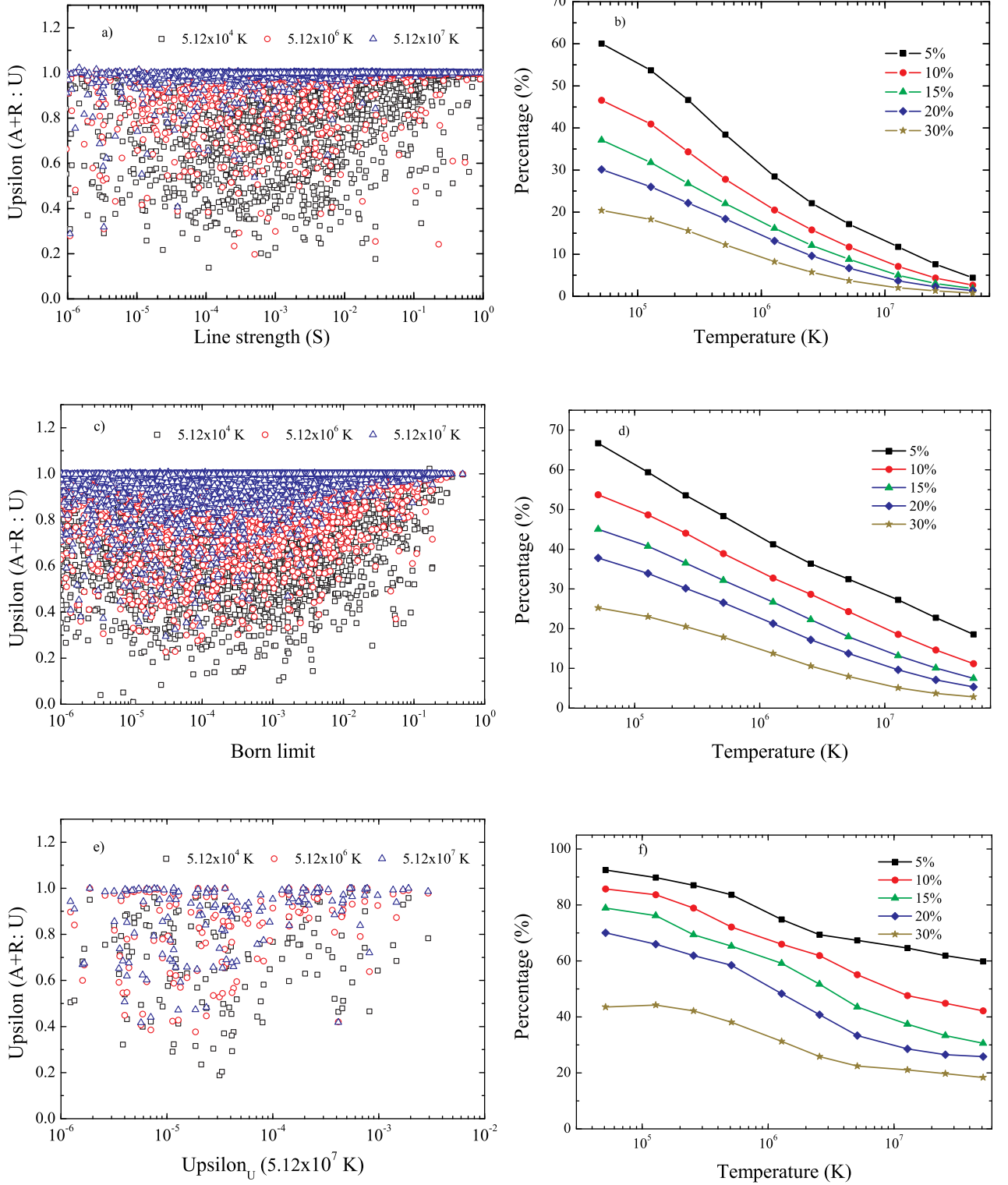


Figure 7. Left-hand panels: Scatter plots showing the ratio of the effective collision strengths (Υ) with Auger-plus-radiation damping ($\Upsilon(A+R)$) to without damping (Υ_U) as a function of a) line strength, c) infinite temperature Born limit, e) undamped Υ at the highest tabulated temperature (5.12×10^7 K), for dipole, non-dipole allowed and forbidden transitions, respectively. Right-hand panels: percentage of corresponding transitions where the effect of damping exceeds 5%, 10%, 15%, 20% and 30% [Galeon online].

Table 1. Energy levels (Ryd), and differences, for the $2s^22p^63l$, $2s^22p^53s3l$ ($l=s, p$ and d), $2s^22p^53p^2$ and $2s^22p^53p3d$ configurations of Fe^{15+} .

Index	Configuration	$^{2S+1}L_J$	NIST ^a	AS ^b	GRASP ^c	FAC ^d	AS-NIST	GRASP -NIST
1	$2s^22p^63s$	$^2S_{1/2}$	0.00000	0.00000	0.00000	0.00000	0.00000	0.00000
2	$2s^22p^63p$	$^2P_{1/2}$	2.52598	2.55904	2.56618	2.54749	0.03306	0.04020
3	$2s^22p^63p$	$^2P_{3/2}$	2.71688	2.76660	2.75486	2.73695	0.04972	0.03798
4	$2s^22p^63d$	$^2D_{3/2}$	6.15562	6.17619	6.19591	6.16930	0.02057	0.04029
5	$2s^22p^63d$	$^2D_{5/2}$	6.18209	6.21736	6.22081	6.19488	0.03527	0.03872
6	$2s^22p^53s^2$	$^2P_{3/2}$	52.60745	52.34842	52.31794	52.41368	-0.25903	-0.28951
7	$2s^22p^53s^2$	$^2P_{1/2}$	53.51871	53.28728	53.24028	53.33365	-0.23143	-0.27843
8	$2s^22p^53s3p$	$^4S_{3/2}$		54.11760	54.08374	54.17677		
9	$2s^22p^53s3p$	$^4D_{5/2}$	54.51199	54.36541	54.32940	54.42627	-0.14658	-0.18259
10	$2s^22p^53s3p$	$^4D_{7/2}$		54.41366	54.38145	54.47648		
11	$2s^22p^53s3p$	$^2P_{3/2}$		54.42411	54.38938	54.48968		
12	$2s^22p^53s3p$	$^2P_{1/2}$	54.68514	54.55154	54.52045	54.61949	-0.13360	-0.16469
13	$2s^22p^53s3p$	$^4P_{5/2}$		54.65336	54.62489	54.72504		
14	$2s^22p^53s3p$	$^2D_{3/2}$	54.79442	54.65685	54.62869	54.73060	-0.13757	-0.16573
15	$2s^22p^53s3p$	$^2S_{1/2}$	55.05876	54.87978	54.84442	54.93987	-0.17898	-0.21434
16	$2s^22p^53s3p$	$^4D_{1/2}$	55.35947	55.26494	55.21306	55.30885	-0.09453	-0.14641
17	$2s^22p^53s3p$	$^4D_{3/2}$	55.48705	55.35890	55.30739	55.40441	-0.12815	-0.17966
18	$2s^22p^53s3p$	$^4P_{1/2}$	55.48705	55.37835	55.33684	55.42804	-0.10870	-0.15021
19	$2s^22p^53s3p$	$^4P_{3/2}$	55.55084	55.47899	55.43583	55.52946	-0.07185	-0.11501
20	$2s^22p^53s3p$	$^2D_{5/2}$		55.47904	55.44467	55.53084		
21	$2s^22p^53s3p$	$^2D_{5/2}$	55.67842	55.54816	55.50469	55.60098	-0.13026	-0.17373
22	$2s^22p^53s3p$	$^2P_{3/2}$	55.85156	55.61425	55.58697	55.67445	-0.23731	-0.26459
23	$2s^22p^53s3p$	$^2P_{1/2}$		56.29895	56.25643	56.34356		
24	$2s^22p^53s3p$	$^2D_{3/2}$	56.65347	56.45616	56.40948	56.49089	-0.19731	-0.24399
25	$2s^22p^53s3p$	$^2S_{1/2}$	57.10911	57.01687	56.99370	57.08592	-0.09224	-0.11541
26	$2s^22p^53p^2$	$^4P_{3/2}$		57.10417	57.06704	57.15630		
27	$2s^22p^53p^2$	$^2P_{1/2}$		57.10468	57.06488	57.15917		
28	$2s^22p^53p^2$	$^4P_{5/2}$		57.17352	57.13944	57.22799		
29	$2s^22p^53p^2$	$^2F_{7/2}$		57.19233	57.14806	57.24427		
30	$2s^22p^53p^2$	$^2P_{3/2}$		57.26544	57.22768	57.32010		
31	$2s^22p^53p^2$	$^2D_{5/2}$		57.38943	57.35118	57.44727		
32	$2s^22p^53p^2$	$^2D_{3/2}$		57.42587	57.39127	57.48631		
33	$2s^22p^53p^2$	$^4P_{1/2}$		57.44009	57.40547	57.49546		
34	$2s^22p^53p^2$	$^4D_{7/2}$		57.45369	57.42105	57.51216		
35	$2s^22p^53p^2$	$^4D_{5/2}$		57.46957	57.43729	57.53005		
36	$2s^22p^53p^2$	$^4D_{1/2}$		57.93100	57.87458	57.96558		
37	$2s^22p^53p^2$	$^4S_{3/2}$		57.96240	57.91773	58.01194		
38	$2s^22p^53s3d$	$^4P_{1/2}$		58.03132	57.93888	58.02976		
39	$2s^22p^53s3d$	$^4P_{3/2}$		58.10048	58.00538	58.09616		
40	$2s^22p^53p^2$	$^2F_{5/2}$		58.18227	58.12751	58.18495		
41	$2s^22p^53p^2$	$^4D_{3/2}$		58.19672	58.09555	58.20798		
42	$2s^22p^53s3d$	$^4F_{9/2}$		58.19737	58.14156	58.21959		
43	$2s^22p^53s3d$	$^4P_{5/2}$	58.25730	58.21984	58.11794	58.23081	-0.03746	-0.13936

Table 1. -continued

Index	Configuration	$2S+1L_J$	NIST	AS	GRASP	FAC	AS-NIST	GRASP -NIST
44	2s ² 2p ⁵ 3s3d	⁴ F _{7/2}		58.24983	58.16102	58.24724		
45	2s ² 2p ⁵ 3p ²	² S _{1/2}		58.26394	58.21189	58.30063		
46	2s ² 2p ⁵ 3s3d	⁴ F _{5/2}	58.37577	58.32413	58.24386	58.32935	-0.05164	-0.13191
47	2s ² 2p ⁵ 3p ²	² D _{3/2}		58.39817	58.36742	58.42791		
48	2s ² 2p ⁵ 3s3d	² D _{3/2}		58.42714	58.34352	58.45325		
49	2s ² 2p ⁵ 3s3d	⁴ D _{7/2}	58.52157	58.47411	58.39564	58.47794	-0.04746	-0.12593
50	2s ² 2p ⁵ 3p ²	² D _{5/2}		58.48076	58.43827	58.50728		
51	2s ² 2p ⁵ 3p ²	² P _{3/2}	58.54891	58.50036	58.42242	58.53072	-0.04855	-0.12649
52	2s ² 2p ⁵ 3s3d	² F _{5/2}		58.50383	58.45493	58.53880		
53	2s ² 2p ⁵ 3s3d	² P _{1/2}	58.53068	58.54673	58.48029	58.56573	0.01605	-0.05039
54	2s ² 2p ⁵ 3s3d	² P _{3/2}	58.64915	58.72397	58.66234	58.74315	0.07482	0.01319
55	2s ² 2p ⁵ 3s3d	⁴ D _{1/2}		58.81395	58.76090	58.83584		
56	2s ² 2p ⁵ 3s3d	⁴ D _{3/2}	58.98632	59.11274	59.04324	59.12033	0.12642	0.05692
57	2s ² 2p ⁵ 3s3d	⁴ F _{3/2}		59.22437	59.14077	59.20637		
58	2s ² 2p ⁵ 3s3d	² F _{7/2}	58.73116	59.22499	59.13497	59.22747	0.49383	0.40381
59	2s ² 2p ⁵ 3s3d	⁴ D _{5/2}	59.25058	59.25061	59.15303	59.23382	0.00003	-0.09755
60	2s ² 2p ⁵ 3s3d	² D _{5/2}	58.90430	59.29565	59.20474	59.28233	0.39135	0.30044
61	2s ² 2p ⁵ 3s3d	² F _{7/2}	59.38727	59.35148	59.25137	59.33262	-0.03579	-0.13590
62	2s ² 2p ⁵ 3p ²	² P _{1/2}		59.41694	59.34593	59.41507		
63	2s ² 2p ⁵ 3s3d	² D _{5/2}	59.37816	59.42156	59.34082	59.42844	0.04340	-0.03734
64	2s ² 2p ⁵ 3p ²	² P _{1/2}		59.52244	59.47971	59.55788		
65	2s ² 2p ⁵ 3p ²	² P _{3/2}		59.59573	59.55298	59.63194		
66	2s ² 2p ⁵ 3s3d	² D _{3/2}		59.73085	59.68822	59.74983		
67	2s ² 2p ⁵ 3s3d	² P _{1/2}	59.90670	59.95897	59.95160	60.01129	0.05227	0.04490
68	2s ² 2p ⁵ 3p3d	⁴ D _{1/2}		60.13369	60.04611	60.13489		
69	2s ² 2p ⁵ 3p3d	⁴ D _{3/2}		60.20690	60.11829	60.19617		
70	2s ² 2p ⁵ 3s3d	² F _{5/2}	59.74267	60.22959	60.12842	60.20705	0.48692	0.38575
71	2s ² 2p ⁵ 3p3d	⁴ D _{5/2}		60.32195	60.23238	60.32059		
72	2s ² 2p ⁵ 3p3d	⁴ G _{7/2}		60.43767	60.35233	60.43839		
73	2s ² 2p ⁵ 3p3d	⁴ G _{9/2}		60.46285	60.37302	60.46292		
74	2s ² 2p ⁵ 3s3d	² P _{3/2}	60.09806	60.46553	60.40230	60.47152	0.36747	0.30424
75	2s ² 2p ⁵ 3p3d	⁴ D _{7/2}		60.47514	60.38502	60.47372		
76	2s ² 2p ⁵ 3p3d	⁴ G _{11/2}		60.50404	60.41011	60.50021		
77	2s ² 2p ⁵ 3p3d	² D _{5/2}		60.52599	60.44777	60.53085		
78	2s ² 2p ⁵ 3p3d	² P _{3/2}		60.57279	60.48675	60.57393		
79	2s ² 2p ⁵ 3p3d	⁴ F _{5/2}		60.63453	60.55605	60.63774		
80	2s ² 2p ⁵ 3p3d	² F _{7/2}		60.63882	60.54820	60.64132		
81	2s ² 2p ⁵ 3p3d	² P _{1/2}		60.69241	60.60183	60.69357		
82	2s ² 2p ⁵ 3p3d	² G _{7/2}		60.74357	60.67077	60.75621		
83	2s ² 2p ⁵ 3p3d	⁴ P _{1/2}		60.83523	60.73533	60.82300		
84	2s ² 2p ⁵ 3p3d	⁴ F _{9/2}		60.84000	60.76830	60.85278		
85	2s ² 2p ⁵ 3p3d	⁴ P _{3/2}		60.86506	60.77171	60.85769		
86	2s ² 2p ⁵ 3p3d	⁴ S _{3/2}		60.90803	60.81615	60.90062		
87	2s ² 2p ⁵ 3p3d	⁴ D _{7/2}		60.92332	60.82874	60.91466		
88	2s ² 2p ⁵ 3p3d	⁴ F _{5/2}		60.94396	60.85344	60.93610		
89	2s ² 2p ⁵ 3p3d	⁴ P _{5/2}		60.95386	60.85914	60.94113		
90	2s ² 2p ⁵ 3p3d	² D _{3/2}		60.98620	60.91494	60.99307		
91	2s ² 2p ⁵ 3p3d	² P _{3/2}		61.05753	60.96448	61.04079		
92	2s ² 2p ⁵ 3p3d	⁴ F _{9/2}		61.06044	60.95573	61.04687		
93	2s ² 2p ⁵ 3p3d	⁴ D _{5/2}		61.09688	61.01801	61.09755		

Table 1. -continued

Index	Configuration	$2S+1L_J$	NIST	AS	GRASP	FAC	AS-NIST	GRASP -NIST
95	2s ² 2p ⁵ 3p3d	² F _{5/2}		61.14734	61.06369	61.14624		
96	2s ² 2p ⁵ 3p3d	⁴ D _{7/2}		61.16998	61.08498	61.16228		
97	2s ² 2p ⁵ 3p3d	² P _{1/2}		61.18777	61.11025	61.18841		
98	2s ² 2p ⁵ 3p3d	² D _{3/2}		61.25489	61.18234	61.26136		
99	2s ² 2p ⁵ 3p3d	⁴ D _{5/2}		61.27670	61.20205	61.28070		
100	2s ² 2p ⁵ 3p3d	² D _{3/2}		61.32968	61.24893	61.32473		
101	2s ² 2p ⁵ 3p3d	⁴ G _{5/2}		61.34088	61.24585	61.33104		
102	2s ² 2p ⁵ 3p3d	⁴ D _{1/2}		61.41249	61.35321	61.42349		
103	2s ² 2p ⁵ 3p3d	² F _{5/2}		61.43393	61.34445	61.42516		
104	2s ² 2p ⁵ 3p3d	² S _{1/2}		61.49422	61.42443	61.48894		
105	2s ² 2p ⁵ 3p3d	⁴ F _{3/2}		61.49958	61.40208	61.50040		
106	2s ² 2p ⁵ 3p3d	⁴ F _{7/2}		61.51701	61.42221	61.50676		
107	2s ² 2p ⁵ 3p3d	² F _{5/2}		61.57211	61.47347	61.55745		
108	2s ² 2p ⁵ 3p3d	² F _{7/2}		61.65079	61.56056	61.64055		
109	2s ² 2p ⁵ 3p3d	² G _{9/2}		61.67835	61.58175	61.66370		
110	2s ² 2p ⁵ 3p3d	⁴ D _{3/2}		61.69701	61.61493	61.68724		
111	2s ² 2p ⁵ 3p3d	² G _{9/2}		61.79328	61.69334	61.76535		
112	2s ² 2p ⁵ 3p3d	⁴ F _{3/2}		61.82696	61.72111	61.80285		
113	2s ² 2p ⁵ 3p3d	² D _{5/2}		61.89847	61.80037	61.87459		
114	2s ² 2p ⁵ 3p3d	² D _{5/2}		61.96161	61.86516	61.93945		
115	2s ² 2p ⁵ 3p3d	⁴ P _{1/2}		61.97606	61.88979	61.96275		
116	2s ² 2p ⁵ 3p3d	² F _{7/2}		61.99048	61.89980	61.96894		
117	2s ² 2p ⁵ 3p3d	² P _{3/2}		62.00886	61.91457	61.98790		
118	2s ² 2p ⁵ 3p3d	⁴ P _{5/2}		62.04487	61.94888	62.02041		
119	2s ² 2p ⁵ 3p3d	⁴ D _{1/2}		62.06520	61.97998	62.05719		
120	2s ² 2p ⁵ 3p3d	⁴ D _{3/2}		62.06835	61.97802	62.06089		
121	2s ² 2p ⁵ 3p3d	² F _{7/2}		62.10521	61.99687	62.07502		
122	2s ² 2p ⁵ 3p3d	² D _{5/2}		62.11542	62.02163	62.09605		
123	2s ² 2p ⁵ 3p3d	² D _{3/2}		62.12317	62.05018	62.11336		
124	2s ² 2p ⁵ 3p3d	² D _{3/2}		62.29418	62.27680	62.32294		
125	2s ² 2p ⁵ 3p3d	² D _{5/2}		62.33871	62.28342	62.34267		
126	2s ² 2p ⁵ 3p3d	² P _{1/2}		62.36979	62.31859	62.37920		
127	2s ² 2p ⁵ 3p3d	² P _{3/2}		62.54002	62.50435	62.55742		
128	2s ² 2p ⁵ 3p3d	² S _{1/2}		62.71307	62.70084	62.74891		
129	2s ² 2p ⁵ 3p3d	² G _{7/2}		62.83419	62.72376	62.79211		
130	2s ² 2p ⁵ 3p3d	² F _{5/2}		62.89339	62.83399	62.88208		
131	2s ² 2p ⁵ 3p3d	⁴ P _{3/2}		62.94192	62.86270	62.92242		
132	2s ² 2p ⁵ 3p3d	² P _{1/2}		63.10850	63.03638	63.08932		
133	2s ² 2p ⁵ 3p3d	² D _{3/2}		63.27928	63.21048	63.29528		
134	2s ² 2p ⁵ 3p3d	² D _{5/2}		63.35811	63.27358	63.36869		

^ahttp://physics.nist.gov/PhysRefData/ASD/levels_form.html

^bAUTOSTRUCTURE (present work).

^cAggarwal and Keenan (2007).

^dPresent work.

Table 2. Electric dipole radiative rates.

i	j	AS ^a	GRASP ^b	FAC ^c
1	2	6.071(09) ^d	6.283(09)	6.303(09)
1	3	7.542(09)	7.834(09)	7.884(09)
1	6	8.553(11)	8.202(11)	6.465(11)
1	7	8.317(11)	8.450(11)	6.666(11)
1	26	9.461(10)	9.327(10)	8.946(10)
1	27	3.088(11)	3.087(11)	2.991(11)
1	30	1.199(11)	1.187(11)	1.188(11)
1	33	8.400(10)	8.529(10)	8.788(10)
1	36	6.020(10)	5.136(10)	6.060(10)
1	37	2.067(10)	1.664(10)	2.180(10)
1	38	4.509(10)	4.774(10)	4.486(10)
1	39	9.727(10)	9.867(10)	9.301(10)
1	41	8.636(09)	6.427(09)	7.977(09)
1	47	2.700(10)	4.872(09)	5.000(10)
1	48	3.379(10)	4.862(10)	5.315(09)
1	51	1.473(10)	5.425(08)	1.757(08)
1	53	1.161(12)	1.025(12)	1.000(12)
1	54	4.042(12)	3.670(12)	3.545(12)
1	55	3.413(12)	3.161(12)	3.205(12)
1	56	1.197(12)	7.926(11)	9.465(11)
1	57	2.133(11)	2.632(11)	2.790(11)
1	62	3.950(11)	5.031(11)	4.780(11)
1	64	7.181(10)	4.447(10)	1.723(11)
1	65	2.730(12)	2.170(12)	3.221(12)
1	66	1.217(13)	1.359(13)	1.145(13)
1	67	2.254(13)	2.461(13)	2.260(13)
1	74	7.338(12)	9.012(12)	8.160(12)

^aAUTOSTRUCTURE (present work).

^bAggarwal and Keenan (2007).

^cPresent work.

^d(m) denotes $\times 10^m$.

Table 3. Excitation energies (Ryd) used for dipole transitions with large differences at low temperatures between the ICFT and DARC effective collision strengths.

i	j	ICFT ^a	DARC ^b	ICFT–DARC
1	6	52.60745	52.31155	0.29589
1	7	53.51871	53.22823	0.29048
2	8	51.74576	51.51313	0.23263
2	11	52.05286	51.83545	0.21741
2	12	52.15916	51.95366	0.20550
2	15	52.53278	52.28154	0.25124
2	17	52.96107	52.73537	0.22570
2	22	53.32558	53.01148	0.31410
2	23	53.92686	53.69872	0.22814
2	24	54.12749	53.85740	0.27009
3	8	51.55486	51.33900	0.21586
3	9	51.79511	51.57144	0.22367
3	11	51.86196	51.62987	0.23209
3	13	52.08980	51.86496	0.22485
3	14	52.07754	51.86496	0.21259
3	15	52.34188	52.10219	0.23969
3	17	52.77017	52.55290	0.21727
3	19	52.91628	52.67441	0.24187
3	22	53.13468	52.82709	0.30759
3	23	53.73596	53.50953	0.22643
3	24	53.93659	53.66709	0.26949
4	6	46.45183	46.11676	0.33507
4	7	47.36309	47.04529	0.31780
5	6	46.42536	46.09344	0.33192

^aPresent work.

^bAggarwal and Keenan (2008).

Table 4. Undamped (U) and Auger-plus-radiation damped (A+R) effective collision strengths $\Upsilon_{i,j}$, at the given temperatures.

i	j	5.12×10^4 K		5.12×10^5 K		5.12×10^6 K	
		U	A+R	U	A+R	U	A+R
1	2	1.38(+0) ^a	1.37(+0)	1.22(+0)	1.22(+0)	1.51(+0)	1.51(+0)
1	3	2.28(+0)	2.30(+0)	2.40(+0)	2.40(+0)	2.99(+0)	2.99(+0)
1	4	1.27(-1)	1.27(-1)	1.28(-1)	1.28(-1)	1.46(-1)	1.43(-1)
1	5	1.90(-1)	1.90(-1)	1.92(-1)	1.92(-1)	2.19(-1)	2.14(-1)
1	6	1.56(-1)	5.25(-2)	8.28(-2)	3.08(-2)	1.64(-2)	9.04(-3)
1	7	8.20(-2)	3.67(-2)	4.12(-2)	1.79(-2)	8.38(-3)	4.87(-3)
1	8	5.58(-2)	3.08(-2)	2.17(-2)	1.43(-2)	6.27(-3)	5.29(-3)
1	9	5.32(-2)	2.88(-2)	2.06(-2)	1.21(-2)	5.56(-3)	4.39(-3)
1	10	5.39(-2)	3.69(-2)	2.12(-2)	1.54(-2)	6.28(-3)	5.48(-3)
1	11	3.14(-2)	1.67(-2)	1.34(-2)	7.34(-3)	4.12(-3)	3.26(-3)
1	12	1.74(-2)	7.07(-3)	7.60(-3)	3.75(-3)	2.13(-3)	1.60(-3)
1	13	3.84(-2)	1.47(-2)	1.45(-2)	7.08(-3)	4.02(-3)	3.03(-3)
1	14	4.00(-2)	1.85(-2)	1.67(-2)	9.85(-3)	4.99(-3)	4.08(-3)
1	15	4.19(-2)	2.27(-2)	1.75(-2)	1.12(-2)	7.94(-3)	7.04(-3)
1	16	1.38(-2)	7.14(-3)	6.78(-3)	3.60(-3)	1.73(-3)	1.25(-3)
1	17	2.66(-2)	1.39(-2)	1.32(-2)	6.97(-3)	3.73(-3)	2.82(-3)
1	18	1.51(-2)	6.32(-3)	7.76(-3)	3.53(-3)	2.21(-3)	1.60(-3)
1	20	2.67(-2)	1.39(-2)	1.46(-2)	7.66(-3)	3.66(-3)	2.61(-3)
1	19	3.71(-2)	2.09(-2)	1.70(-2)	1.02(-2)	5.99(-3)	5.00(-3)
1	21	4.38(-2)	2.24(-2)	1.94(-2)	9.99(-3)	5.69(-3)	4.34(-3)
1	22	3.45(-2)	1.46(-2)	1.59(-2)	7.09(-3)	3.53(-3)	2.26(-3)
1	23	3.86(-2)	2.63(-2)	3.22(-2)	2.30(-2)	1.90(-2)	1.75(-2)
1	24	2.42(-2)	1.10(-2)	1.02(-2)	5.86(-3)	3.22(-3)	2.62(-3)
1	38	7.23(-3)	3.76(-3)	2.95(-3)	1.83(-3)	1.41(-3)	1.27(-3)
1	39	4.26(-3)	2.46(-3)	2.36(-3)	1.76(-3)	1.73(-3)	1.65(-3)
1	25	9.07(-2)	8.37(-2)	8.61(-2)	8.08(-2)	8.35(-2)	8.26(-2)
1	43	7.58(-3)	4.53(-3)	2.15(-3)	1.13(-3)	2.98(-4)	1.71(-4)
1	42	6.52(-3)	3.70(-3)	3.23(-3)	2.05(-3)	1.23(-3)	1.08(-3)
1	44	7.51(-3)	3.65(-3)	3.01(-3)	1.79(-3)	1.44(-3)	1.30(-3)
1	46	6.50(-3)	3.02(-3)	2.49(-3)	1.31(-3)	6.90(-4)	5.45(-4)
1	48	5.04(-3)	1.88(-3)	1.35(-3)	4.82(-4)	1.84(-4)	7.99(-5)
1	53	3.10(-3)	1.27(-3)	1.13(-3)	6.25(-4)	5.14(-4)	4.53(-4)
1	49	5.05(-3)	2.67(-3)	1.65(-3)	8.32(-4)	3.54(-4)	2.52(-4)
1	52	5.34(-3)	2.47(-3)	1.70(-3)	7.64(-4)	3.08(-4)	1.93(-4)
1	54	3.65(-3)	1.47(-3)	1.21(-3)	6.31(-4)	4.50(-4)	3.82(-4)
1	58	5.18(-3)	2.01(-3)	1.81(-3)	9.03(-4)	5.36(-4)	4.29(-4)
1	55	6.96(-3)	5.05(-3)	4.61(-3)	4.11(-3)	2.80(-3)	2.74(-3)
1	59	1.17(-2)	9.16(-3)	8.58(-3)	7.80(-3)	5.53(-3)	5.44(-3)
1	56	5.52(-3)	2.43(-3)	2.39(-3)	1.38(-3)	8.74(-4)	7.50(-4)
1	57	4.91(-3)	1.66(-3)	1.94(-3)	8.33(-4)	5.58(-4)	4.21(-4)
1	60	1.27(-2)	9.56(-3)	9.18(-3)	8.14(-3)	5.29(-3)	5.16(-3)
1	63	1.31(-2)	1.04(-2)	9.78(-3)	8.92(-3)	5.89(-3)	5.79(-3)
1	61	1.01(-2)	7.06(-3)	6.92(-3)	6.00(-3)	4.13(-3)	4.02(-3)
1	66	1.65(-3)	5.00(-4)	5.56(-4)	1.51(-4)	7.43(-5)	2.45(-5)
1	70	9.28(-3)	5.77(-3)	5.58(-3)	4.62(-3)	3.36(-3)	3.25(-3)
1	67	5.48(-3)	1.67(-3)	1.82(-3)	8.44(-4)	5.88(-4)	4.73(-4)
1	74	5.77(-3)	3.10(-3)	3.20(-3)	2.45(-3)	1.71(-3)	1.62(-3)